

# Structure Optimization for Cellulose-Based Separator through Fiber Size Regulation for High Performance Lithium Metal Batteries

Zhenghao Li,<sup>[a, b]</sup> Zongtao Lu,<sup>[b]</sup> Tianyou Zhang,<sup>[b]</sup> Bingsen Qin,<sup>[b]</sup> Wei Yan,<sup>[b]</sup> Li Dong,<sup>[c]</sup> Jie Dong,<sup>[d]</sup> Chunxiang Ma,<sup>[d]</sup> Zhiping Chen,<sup>[d]</sup> Wei Li,\*<sup>[a]</sup> Yun Zheng,\*<sup>[b]</sup> and Jiujun Zhang\*<sup>[b]</sup>

Cellulose-based separator exhibits excellent electrolyte affinity, thermal stability, and mechanical strength, which acts as a promising alternative to commercial polyolefin separators in lithium metal batteries (LMBs). Fiber size in cellulose-based separators plays a crucial role in determining their physicochemical structure and mechanical strength, as well as the electrochemical performance of corresponding LMBs. Herein, the fiber size in cellulose-based separators was first time regulated to optimize their mechanical stability and the related battery performance. The influences of fiber size in the separator on chemical structure, mechanical properties, surface morphology, electrochemical behavior were investigated in

detail, in which the underlying mechanism between separator structure and the related performance was elucidated. As a result, the separator optimized by fiber size regulation exhibited excellent thermal stability under 180 °C, good tensile strengths of 6.0 MPa and Young's moduli of 315.9 MPa, superior room temperature ionic conductivity of 1.87 mS cm<sup>-1</sup>, as well as significantly improved electrochemical performance of corresponding batteries. It can be concluded that structure optimization for cellulose-based separator through fiber size regulation is an effective and indispensable approach towards high safety and high performance LMBs.

## 1. Introduction

In recent years, there has been a notable resurgence of interest in lithium (Li) metal batteries (LMBs) within both academia and industry. This increasing attention is primarily attributed to their significantly higher energy density compared to state-of-the-art lithium-ion batteries (LIBs) that utilize graphite anodes.<sup>[1]</sup> Despite the enormous application potential of LMBs in consumer electronics, electric vehicles, and large energy storage facilities, the inherent instability of Li metal has presented challenges in terms of safety and cycle-life for LMBs.<sup>[2]</sup> These challenges have greatly hindered the large-scale commercialization of LMBs.

As a crucial component of LMBs to overcome above challenges, separator not only isolates the Li metal anode and cathode to prevent short circuits, but also serves as an electrolyte reservoir during charging/discharging, facilitating Li<sup>+</sup> migration and transformation for high-performance batteries.<sup>[3]</sup> However, current commercially available polyolefin separators suffer from limitations such as inadequate wettability of the electrolyte, insufficient porosity, discontinuous pore configuration, unreactive surface groups and thermal shrinkage at high temperatures, leading to their suboptimal compatibility with Li metal anode.<sup>[4]</sup> With respect to this, there has been a focus on cellulose-based separators in recent year for their superior electrolyte affinity, abundant pore architecture, and exceptional thermal stability, leading to excellent electrochemical performance and safety, is widely used as the primary matrix for separators.<sup>[5]</sup>

Among current works about this type of advanced separators, structure optimization is recognized as one of the most effective approaches for performance promotion.<sup>[5c,6]</sup> Specially, it is known that fiber size in separators plays a crucial role in determining their pore structure, mechanical strength, electrolyte uptake, and retention, all of which significantly impact the electrochemical performance of LMBs when assembled. To be specific, larger fiber typically lead to a rougher surface, increased thickness, and decreased strength of the separator, ultimately harming its electrochemical and mechanical properties. Conversely, excessively small fiber sizes can cause the separator to be overly dense, hindering the transmission path of Li<sup>+</sup> ions and thus affecting electrochemical performance, while also raising the complexity and cost of the production process for the separator (Figure 1b).

[a] Z. Li, W. Li

Guangxi Key Laboratory of Clean Pulp & Papermaking and Pollution Control, College of Light Industry and Food Engineering, Guangxi University, Nanning 530004, China  
E-mail: weili@gxu.edu.cn

[b] Z. Li, Z. Lu, T. Zhang, B. Qin, W. Yan, Y. Zheng, J. Zhang

Institute of New Energy Materials and Engineering/School of Materials Science and Engineering, Fuzhou University, Fuzhou 350108, China  
E-mail: yunzheng@fzu.edu.cn  
jiujun.zhang@fzu.edu.cn

[c] L. Dong

Zhaoqing Leoch battery Technology Co., Ltd, Guangdong Province, 518000, P. R. China

[d] J. Dong, C. Ma, Z. Chen

Anhui Leoch Renewable Energy Development Co., Ltd, Huaibei City 235000, China

 Supporting information for this article is available on the WWW under <https://doi.org/10.1002/batt.202400435>

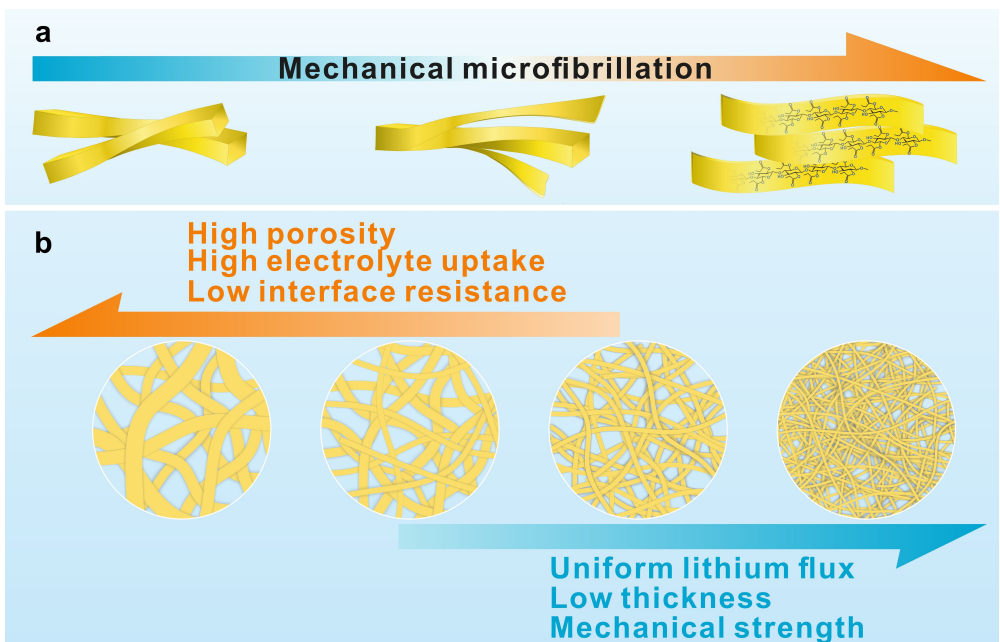


**Figure 1.** Design of cellulose-based separators. Schematic illustration for (a) morphology and size regulation through mechanical treatment, and (b) cellulose-based separators with various fiber sizes towards different potential properties.

Therefore, in order to achieve high electrochemical performance and good safety LMBs assembled with cellulose-based separator, it is necessary to modulate the separators' fiber size and further study the corresponding structure-function relationship. However, the research in this regard is currently rarely explored, the influence of fiber size on the physical and electrochemical properties of such advanced separators and related LMBs has not been comprehensively investigated.

Accordingly, basing on our previous work about a proposed PCF separator for LMBs,<sup>[7]</sup> structure optimization for cellulose-based separator through fiber size regulation was performed enabling high performance LMBs in this research. Specifically, cellulose-based separators with various fiber sizes were first fabricated though different mechanical microfibrillation (Figure 1a). Then, the impact of fiber size on separators' physicochemical structures and properties, as well as batteries' electrochemical performance was further investigated through various physicochemical characterizations and electrochemical testing. The results indicate that fiber size regulation could significantly promote the mechanical strength of cellulose-based separators, as well as the Li flux, Li deposition behavior, rate performance, and cycle life of LMBs. As for the batteries paired with LiPF<sub>6</sub> (LFP) cathode, an initial discharge capacity of 149.8 mAhg<sup>-1</sup> and a capacity retention rate of 84.4% after 300 cycles was achieved after fiber size regulation. This study not only marks a milestone in understanding the structure-activity relationship of cellulose-based separators for LMBs, but also offers valuable insights and guidance for future research on separators to tackle the key challenges of LMBs.

## 2. Results and Discussion

### 2.1. Physicochemical Characterizations

Four types of cellulose fiber (CF) with different size were prepared though different mechanical treatment, named CF1, CF2, CF3, and CF4 according to their sizes from largest to smallest. Those CFs further modified to obtain propionylated cellulose fiber (PCF), named as PCF1, PCF2, PCF3, PCF4. More details about fabrication and related discussion about process parameters including beating degree (Figure S1), length-diameter ratio (Table S1), and substitution degree of propionylated fiber (Figure S2) are presented in Supporting Information (SI).

Physicochemical structure of these separators was analyzed using X-ray diffraction analysis (XRD), infrared (IR) spectroscopy, X-ray photoelectron spectroscopy (XPS), and so on. As for crystal structure, it is known that the lower the crystallinity of the cellulose-based battery separators, the faster the diffusion rate of Li<sup>+</sup> will be.<sup>[8]</sup> Figure 2a illustrates the XRD patterns of propionylated fibers of varying sizes, showing signal peaks corresponding to the (101) and (002) lattice planes at 18° and 22.5°, indicating typical cellulose I crystals.<sup>[9]</sup> The crystallinity percentages of PCF1, PCF2, PCF3, and PCF4 are 72.6%, 72.2%, 67.7%, and 67.0%, respectively. It is evident that the crystallinity of the sample slightly decreases with decreasing fiber size. This phenomenon may be attributed to the increase in specific surface area of the fibers, leading to a higher amount of propionyl groups grafted onto the fibers, consequently causing more damage to the crystalline zone of the fibers.<sup>[10]</sup>

In addition to the crystal structures, the chemical structure and bonding environment of those four main samples were further characterized through IR spectroscopy and XPS. In

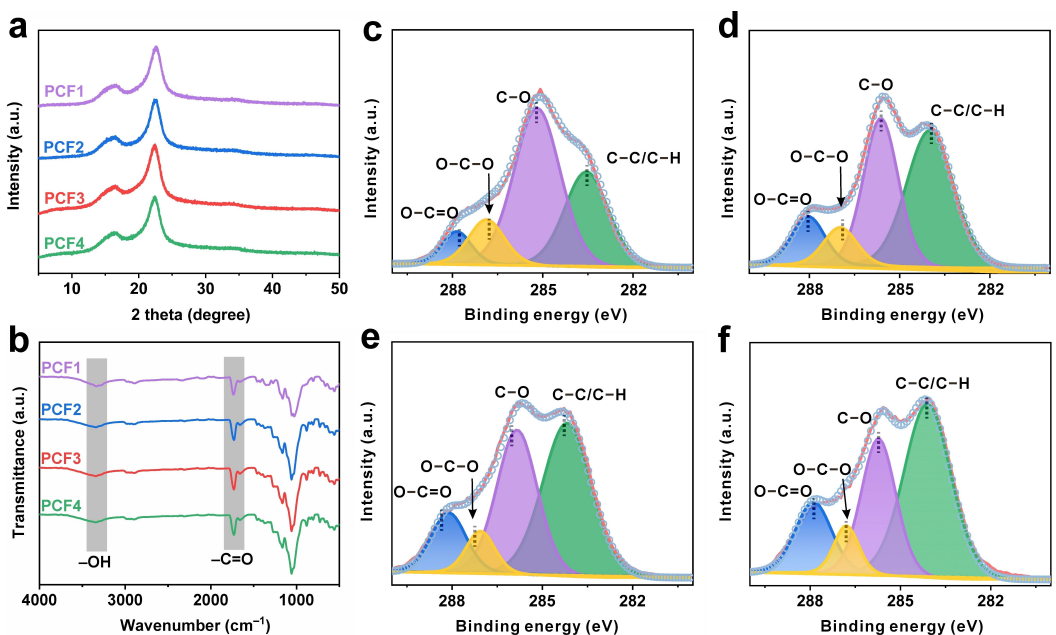


**Figure 2.** Physicochemical structure of separators with different fiber sizes. (a) XRD spectra of propionylated fibers. (b) ATR-FTIR spectra and (c-f) high-resolution C 1s XPS deconvolution spectra of propionylated fibers (c: PCF1, d: PCF2, e: PCF3, f: PCF4).

Figure 2b, signal peaks corresponding to  $-\text{OH}$  group and  $\text{O}-\text{C}=\text{O}$  group are observed at  $3300 \text{ cm}^{-1}$  and  $1740 \text{ cm}^{-1}$  respectively in propionylated fibers. Notably, the signal intensity of  $\text{O}-\text{C}=\text{O}$  group slightly increases with decreasing fiber size.<sup>[11]</sup> Figure 2b-e displays high-resolution C 1s XPS spectra of propionylated fibers. The data reveals that the peak associated with  $\text{O}-\text{C}=\text{O}$  at  $287.9 \text{ eV}$  is presented in all samples, suggesting the occurred propionylation reaction. Furthermore, as the fiber size decreases from PCF1 to PCF4, the signal peak area of the  $\text{C}-\text{C/C-H}$  structure at  $283.9 \text{ eV}$  increases from  $25.4\%$  to  $49.3\%$ , while the proportion of the  $\text{C}-\text{O}$  structure at  $285.5 \text{ eV}$  decreases from  $56.7\%$  to  $28.29\%$ .

These findings align with the results obtained from above mentioned degree of substitution (DS) value calculation, as well as the XRD and IR spectrum analysis, suggesting that propionyl chloride has been effectively bonded to fibers of varying sizes, and the fiber size decreases with the degree of grafting escalating. This is attributed to a higher specific surface area caused from decreased fiber size, which exposes more hydroxyl groups on the fiber surface. As a result, the accessibility of propionylation reactions is enhanced, leading to much more grafted propionyl groups.

In addition to above basic physicochemical characterizations, some physical properties including thermal stability and mechanical strength have been further involved subsequently. In general, separators with high thermal stability offer enhanced safety for LMBs.<sup>[12]</sup> Figure 3a displays thermogravimetric analysis (TGA) results of PCF separators with varying fiber sizes. The thermal decomposition process of the separators can be divided into two main stages, the first stage occurs at  $100\text{--}150^\circ\text{C}$ , with slight mass loss caused from water evaporation in the separators, the second stage takes place at  $270\text{--}355^\circ\text{C}$ , with

rapid mass decrease primarily due to cellulose thermal decomposition.<sup>[13]</sup> The initial thermal decomposition temperature ( $278^\circ\text{C}$ ) of the PCF separators remains consistent across different fiber sizes in the second stage, indicating small impact of fiber size on thermal stability of separators.

Thermal dimensional stability test is another widely recognized method to evaluate separators' thermal stability.<sup>[14]</sup> Figure 3b demonstrates that the size shrinkage rate of PCF separators with different fiber sizes is less than  $5\%$  after being subjected to  $180^\circ\text{C}$  for 15 minutes, indicating their excellent thermal dimensional stability.<sup>[15]</sup> This desirable performance can be mainly attributed to the exceptional inherent thermal stability of cellulose. Moreover, this outcome provides additional evidence that the fiber size also has small impact on the thermal stability of cellulose-based separators.

In addition to thermal stability, excellent mechanical strength is crucial for preventing deformation or breakage of the separator during operation, which is a key physical property that significantly impacting battery safety.<sup>[16]</sup> With respect to this, Figure 3c illustrates stress-strain curves of PCF separators, and Table S2 presents a summary of the related tensile strength and Young's modulus values. The tensile strengths of PCF1, PCF2, PCF3, and PCF4 separators were  $1.4 \text{ MPa}$ ,  $2.0 \text{ MPa}$ ,  $6.0 \text{ MPa}$ , and  $8.1 \text{ MPa}$ , respectively, with corresponding Young's moduli of  $56.0 \text{ MPa}$ ,  $133.3 \text{ MPa}$ ,  $315.9 \text{ MPa}$ , and  $368.2 \text{ MPa}$ , respectively.

These results clearly indicate that the mechanical strength of the modified separators increases progressively as the fiber size decreases. This enhancement can be attributed to two main factors, including that (1) the reduction in fiber size leads to the Campbell effect during drying process, resulting in tighter fiber connections due to capillary action and mechanical interlocking of microfibers, ultimately improving the mechanical

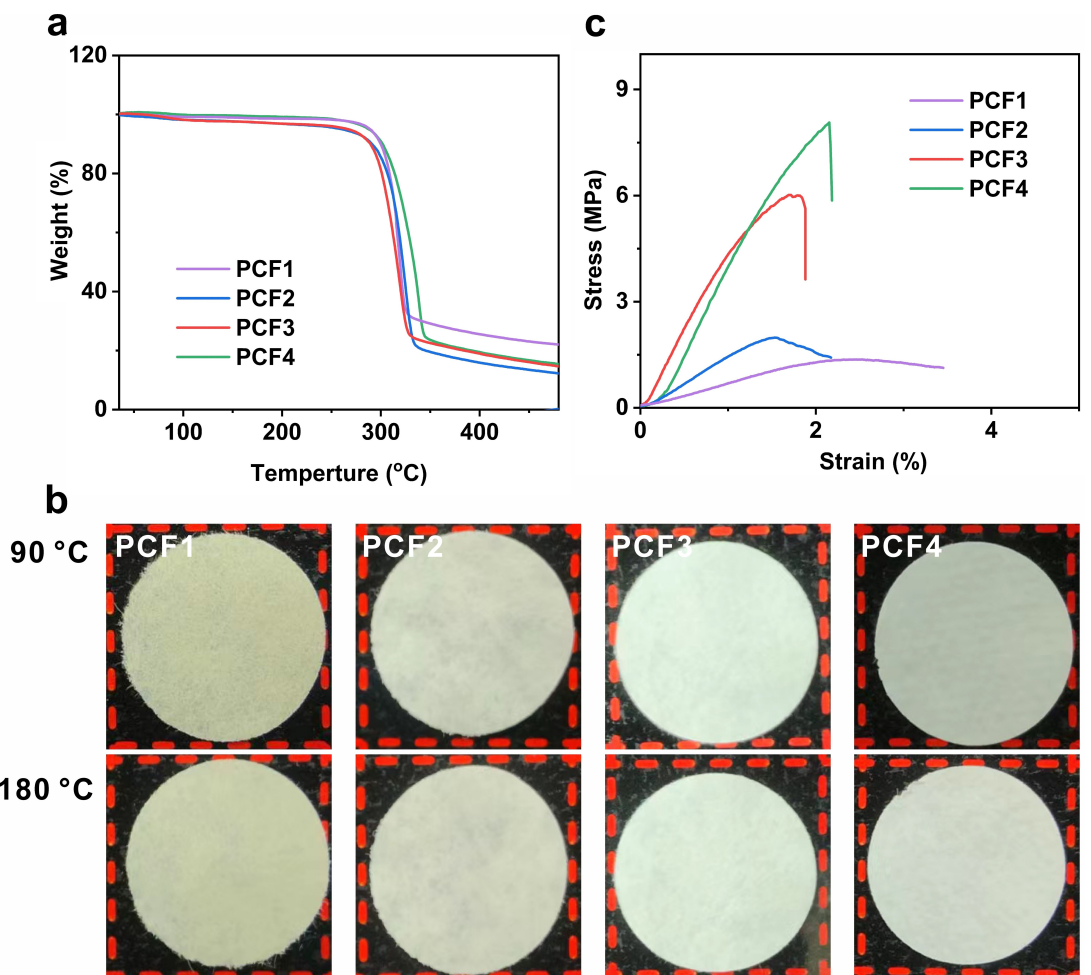


**Figure 3.** Physical properties of PCFs with different fiber sizes. (a) Thermogravimetric analysis (TGA) curves of PCF separators. (b) Optical pictures of PCF separators after storage at 90 °C and 180 °C for 15 min. (c) State-tensile curves of PCF separators.

strength,<sup>[17]</sup> and (2) smaller propionylated fibers exhibit better dispersion in ethanol, thus an improved homogeneity of separators was achieved during vacuum filtration, leading to increased mechanical strength.<sup>[18]</sup>

## 2.2. Morphologies and Structural Features

In addition to the physicochemical characterizations, morphology and structural features of cellulose-based separators have also been analyzed basing on mean surface roughness, pore size distribution, and surface morphology. Specifically, surface roughness of cellulose-based separator reflects the compactness of the separator structure and affects the interface contact effect between the separators and electrodes.<sup>[14,19]</sup> An optical profiler was used to reflect the surface roughness of PCF separators with different fiber sizes, the resulting 3D model photos are shown in Figure 4a-d, while the average roughness values for PCF1, PCF2, PCF3, and PCF4 separators are 6.1 μm, 5.2 μm, 5.0 μm, and 3.6 μm, respectively (Figure S3). It is evident that the average roughness decreases in PCF separators as the fiber size decreases. This reduction is attributed to the decrease

in fiber diameter, leading to increased homogeneity and density of the separator.

Maintaining a submicron pore size distribution in separators is crucial for balancing the electrochemical performance and stability of LMBs. An excessively large separator pore can increase cathode-anode contact, impacting battery safety and cycle life, while an overly dense pore structure can increase internal resistance, limiting Li<sup>+</sup> migration.<sup>[20]</sup> Herein, the pore structure of the diaphragm was analyzed considering two aspects of pore size distribution and porosity. The average pore sizes of PCF1, PCF2, PCF3, and PCF4 separators were measured at 2.79 μm, 1.14 μm, 0.80 μm, and 0.16 μm, respectively. The SEM images confirm that the PCF1 separator contains numerous pores larger than 1 μm in diameter, suggesting possible limitations in its use for LMB applications.<sup>[6b]</sup> As the fiber size decreases, the proportion of submicron-sized pores in the separators gradually increases, leading to a more uniform and denser structure with smaller pore diameters.

Furthermore, porosity and permeability reflect the permeability and pore connectivity of separators, which will affect the Li<sup>+</sup> migration rate.<sup>[6b]</sup> The permeability of separators can be characterized by Gurley number, in which the lower Gurley

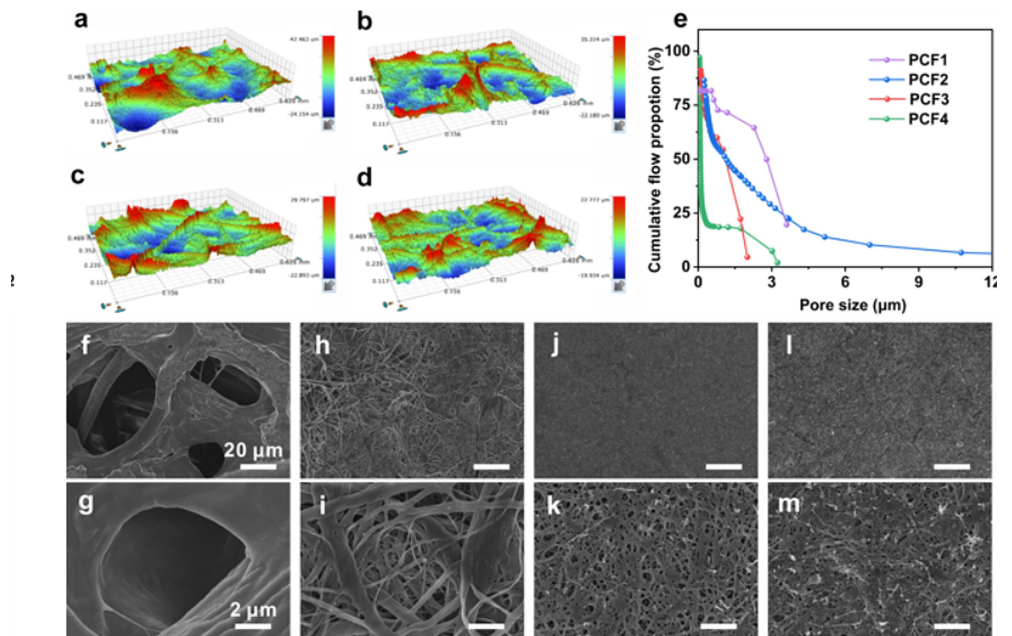


**Figure 4.** Morphologies and structural features of PCF separators with different fiber sizes. (a–d) 3D topography images of PCF separators (a: PCF1 separator, b: PCF2 separator, c: PCF3 separator, d: PCF4 separator) from AFM. (e) Pore size distribution of PCF separators. (f–m) SEM images of PCF separators (f–g: PCF1, h–i: PCF2, j–k: PCF3, l–m: PCF4).

number indicates a higher permeability of the separators. Figure S4 shows the porosity and Gurley number of the PCF separators, the porosities of PCF1, PCF2, PCF3 and PCF4 separators are 77.5%, 73.3%, 67.2% and 57.1%, respectively. The Gurley numbers are 8.5 s 100cc<sup>-1</sup>, 31.5 s 100cc<sup>-1</sup>, 111.0 s 100cc<sup>-1</sup> and 184.5 s 100cc<sup>-1</sup>, respectively. These results reveal that the PCF separators with smaller fiber size possess lower permeability.

SEM images in Figure 4f–m describe the microscopic morphology of PCF separators with different fiber sizes. The PCF1 separator exhibits a dense distribution of micron-sized pores, some exceeding 5 μm in diameter. These micropores pose a risk to battery longevity and safety due to the increased likelihood of direct cathode-anode contact in the event of a short circuit. Moreover, larger pore size compromises the mechanical integrity of the separators, making them more susceptible to penetration by impurities or Li dendrites.<sup>[6b]</sup> While the PCF2 separator still contains some pores at the micron level, the PCF3 and PCF4 separators predominantly have pores at the sub-micron level. The pore distribution is generally homogeneous, effectively inhibiting dendrite formation.<sup>[19]</sup> However, the pore ratio of PCF4 separator decreased significantly compared with that of PCF3 one, which would reduce their electrolyte uptake.

In brief, the PCF separators' pore structure may be efficiently altered by adjusting the fiber size. The PCF3 separator seem to have the most suitable pore structure for the fast lithium transformation and uniform deposition.

### 2.3. Basic Performance of PCF Separators

The fiber size plays a crucial role in determining the structure of the separator. Accordingly, we subsequently focused on studying how this structural variation affects the basic electrolyte uptake/retention and electrochemical performance.

The electrolyte uptake and electrolyte retention of separators are closely related to their pore structure and hydrophilicity.<sup>[21]</sup> As shown in Figure 5a, the electrolyte uptake of PCF1, PCF2, PCF3, and PCF4 separators are 791.2 wt%, 701.6 wt%, 597.9 wt%, and 468.4 wt%, respectively, which shows a significant decreasing trend. This is due to the decrease in fiber size and the subsequently lowered porosity and reduced space for storing electrolyte.

As shown in Figure 5b, the electrolyte retention of PCF1, PCF2, PCF3, and PCF4 separators are 60.1 wt%, 63.1 wt%, 64.5 wt%, and 69.0 wt%, respectively. The modified separators exhibit an increasing trend in electrolyte retention as fiber size decreases. This phenomenon can be interpreted as the higher internal curvature of PCF separators with smaller fiber sizes, resulting in a slower volatilization rate of the electrolyte.

Given the substantial influence of fiber size on the pore structure and electrolyte absorption capacity of cellulose-based separators, an analysis has been further conducted on the ionic conductivity of these separators. Figure 5c shows the Nyquist plots of PCF separators with different fiber sizes at room temperature. Table S3 summarize the thickness, internal resistance and the calculated ionic conductivity ( $\sigma$ , mS cm<sup>-1</sup>). The thickness of PCF1, PCF2, PCF3 and PCF4 separators are 110 μm, 94 μm, 90 μm and 88 μm, respectively, while their  $\sigma$  are 3.31 mS cm<sup>-1</sup>, 2.25 mS cm<sup>-1</sup>, 1.87 mS cm<sup>-1</sup> and 1.63 mS cm<sup>-1</sup>, respectively. The  $\sigma$  of the separators decreases gradually with

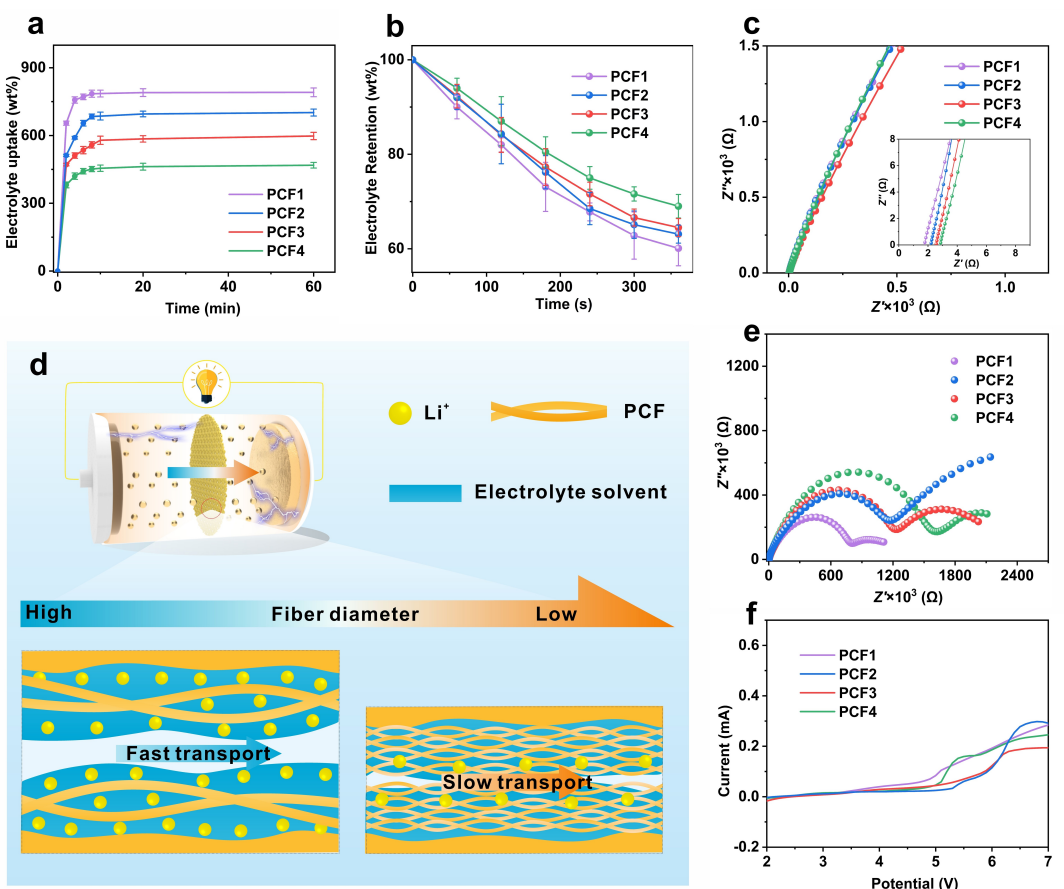


**Figure 5.** Basic performance of PCF separators with different fiber sizes. (a) Electrolyte uptake and (b) electrolyte retention of PCF separators with time. (c) Nyquist plots of PCF separators. (d) The effect of fiber size on the  $\text{Li}^+$  conduction. (e) Nyquist plots of Li/Li battery assembled with PCF separators. (f) LSV curves of Li/SS (stainless steel) battery assembled with PCF separators at a scan rate of 5 mV s<sup>-1</sup>.

reduced fiber size, which is primarily due to the reduced electrolyte uptake and increased internal resistance of these separators. With respect to this, Figure 5d presents a schematic to illustrate the impact of fiber size on the  $\text{Li}^+$  conduction rate in this PCF system. The reduction in fiber size leads to a decrease in separators thickness and a shorter ion transport path. However, it also results in lower porosity and electrolyte uptake of the separators. Based on the findings of the ionic conductivity results, it is suggested that porosity and electrolyte uptake play crucial roles in this regard.

Fiber size not only impacts the  $\text{Li}^+$  transport impedance within the cellulose-based separator, but also influences the impedance between electrolyte and electrode. The Nyquist curve depicted in Figure 5e illustrates that the reduced electrolyte absorption in the separator with smaller fiber size leads to a decreased  $\text{Li}^+$  transfer rate between the separator and electrode. The interfacial resistance of Li/Li batteries assembled with PCF1, PCF2, PCF3, and PCF4 separators was measured at 819.2 Ω, 1040.0 Ω, 1235.8 Ω, and 1688.1 Ω, respectively, showing a gradual increasing trend.<sup>[6b,22]</sup>

After evaluation of ionic conduction for those PCF systems, the electrochemical stability is also significant towards high-performance batteries with better cathode suitability, which is usually evaluated through electrochemical stability window.<sup>[23]</sup>

Figure 5f presents the LSV curve of PCF separators. The rapid increase in current during the steady-state voltage forward scan indicates an electrochemical reaction between the separator and electrolyte. The electrochemical stability windows of PCF1, PCF2, PCF3, and PCF4 separators are 4.6 V, 5.3 V, 5.1 V, and 5.0 V, respectively.<sup>[24]</sup>

#### 2.4. Electrochemical Performance of the LMBs

The electrochemical stability and  $\text{Li}^+$  deposition behavior of PCF system with various separators have been preliminarily compared in long-term Li plating/stripping, in which the battery with Celgard (polypropylene, PP) separator was performed as a general contrast. As compared in Figure 6a–b, a rapid rise in short-circuit polarization voltage can be observed in Li/PP/Li cell, ultimately resulting in a short circuit after 520 hours. As for PCF systems, the presence of numerous micron-sized pores in PCF1 and PCF2 separators results in an uneven  $\text{Li}^+$  deposition and rapid dendrite growth, ultimately leading to short circuits or heightened polarization. Meanwhile, the low electrolyte uptake rate and ion conductivity of the PCF4 separator also contribute to increased polarization in Li/PCF4/Li cell. In contrast, the PCF3 separator demonstrates more stable lithium

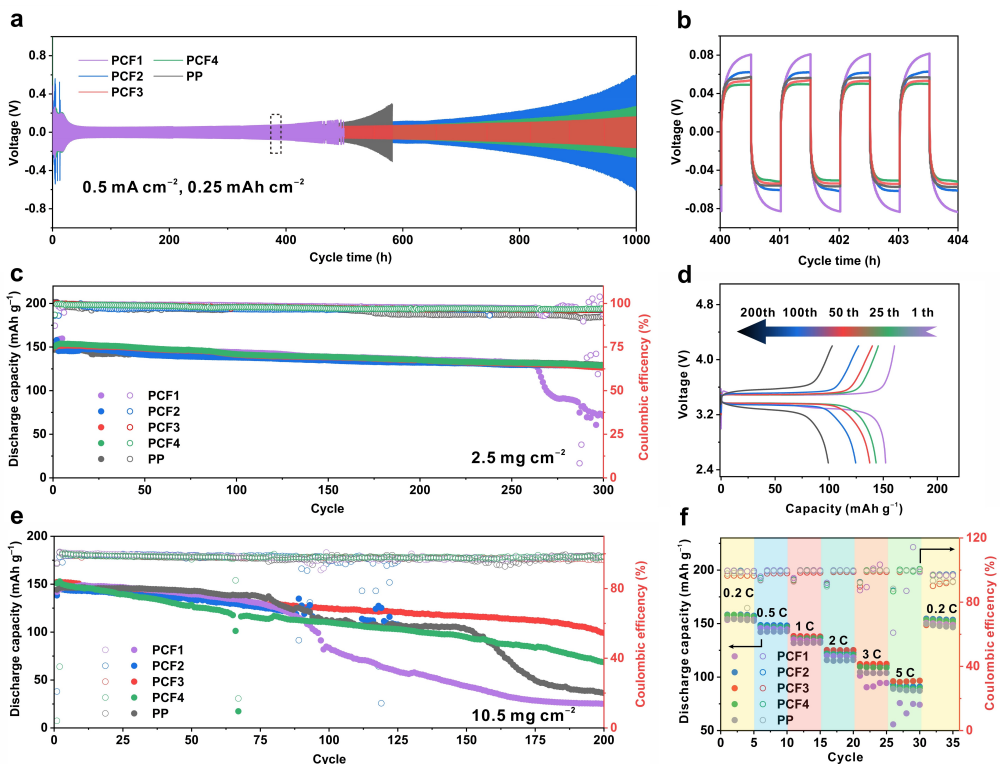


**Figure 6.** Electrochemical performance of the LMBs with PCF separators. (a–b) Galvanostatic cycle curves of Li/PCF separator/Li at  $0.5 \text{ mA cm}^{-2}$ . (c) Cycle performance of Li/PP or PCF separator/LFP (LiPF<sub>6</sub>) at  $0.5 \text{ C}$  (LFP loading is  $2.5 \text{ mg cm}^{-2}$ ). (d) Charge/discharge curves of Li/PCF3 separator/LFP at  $0.5 \text{ C}$ . (e) Cycle performance of Li/PP or PCF separator/LFP at  $0.5 \text{ C}$  (LFP loading is  $10.5 \text{ mg cm}^{-2}$ ). (f) Rate performance of Li/PP or PCF separator/LFP (LFP loading is  $2.5 \text{ mg cm}^{-2}$ ).

plating/stripping behavior and exhibits a lower polarization voltage of 66.5 mV after 500 hours cycling.

Subsequently, the corresponding full batteries with different separators were tested for further performance evaluation. As presented in Figure 6c, the initial discharge specific capacity of Li/PP/LFP is  $146.9 \text{ mAh g}^{-1}$ , decreasing to  $129.4 \text{ mAh g}^{-1}$  after 300 cycles. However, the Coulombic efficiency of this battery decreases after 175 cycles, resulting in an average efficiency of 95.5%. As for the battery with PCF1 separator, a rapid discharge capacity decline and unstable coulombic efficiency can be observed after 264 cycles. On the other hand, the Li/LFP cells with PCF2, PCF3, or PCF4 separators have completed 300 cycles with capacity retention of 84.6%, 84.4%, or 85.8%, respectively. By comparison, micron-sized pores in the PCF1 separator cause short circuits, while batteries with PCF2, PCF3, and PCF4 separators exhibit similar cycling performance, likely due to low Li<sup>+</sup> participation and slow dendrite growth at low current densities, enabling these separators to roughly meet battery cycling requirements.

Next, SEM images of the lithium metal surface were analyzed after 200 hours cycling with PP and PCF3 separator (Figure S6). The results indicate that, in comparison to the PP separator, the Li metal surface associated with the PCF3 separator is notably smoother and flatter. This improvement can be attributed to the more uniform pore distribution and higher ionic conductivity of the PCF3 separator, which effectively reduces the concentration gradient of ions at the

interface. Consequently, the lithium flux is more evenly distributed across the Li metal surface when utilizing the PCF3 separator, mitigating the formation of lithium dendrites.

When it comes to much higher cathode loading ( $10.5 \text{ mg cm}^{-2}$ ) in LMBs, the batteries undergo higher current density, which place greater demands on the structure of separators. The performance difference of these five types of batteries has increased significantly under such running condition. To be specific, Figure 6e reveals that the capacity of Li/PP/LFP dropped significantly to  $36.4 \text{ mAh g}^{-1}$  after 200 cycles. A short circuit after 90 cycles can be found in Li/PCF1 separator/LFP, resulting in a capacity retention of only 17.7% after 200 cycles. The Li/PCF2 separator/LFP experienced irreversible short circuiting after 125 cycles, and the Li/PCF4 separator/LFP maintained a capacity retention of 45.5% after 200 cycles. Compared to these four batteries, the Li/PCF3 separator/LFP shows a higher capacity retention of 65.2% after 200 cycles, illustrating a smooth charge and discharge curve as presented in Figure 6d.

This performance can be attributed to the low ionic conductivity of the PP separator, which leads to increased polarization in the assembled battery and subsequent capacity loss. The micron-sized pores in the PCF1 and PCF2 separators are insufficient to completely prevent the migration of active materials, resulting in short circuits in the batteries constructed with these separators. Conversely, the PCF3 separator features a pore size and distribution that are well-suited for LMB

applications, along with good mechanical strength. Additionally, it possesses higher porosity and liquid absorption capacity, which effectively mitigates battery polarization under high current density, thereby enhancing cycle performance. In contrast, the lower porosity and liquid absorption rate of the PCF4 separator increase the internal resistance of the separator and exacerbate battery polarization, resulting in poorer cycle stability compared to the PCF3 separator.

To further improve the evaluation requirements for battery, rate performance from 0.2 C to 5 C regarding those five types of batteries have been further performed accordingly.<sup>[25]</sup> As shown in Figure 6f and Figure S7, the discharge capacities of the batteries with PP, PCF1, PCF2, PCF3, or PCF4 separators at 5 C are 89.1 mAh g<sup>-1</sup>, 55.8 mAh g<sup>-1</sup>, 92.7 mAh g<sup>-1</sup>, 96.1 mAh g<sup>-1</sup> and 90.6 mAh g<sup>-1</sup> respectively. It can be seen that the Li/PCF3 separator/LFP has the best rate performance, which can be interpreted as its optimal pore distribution and good ion conductivity, further reducing the internal concentration polarization in LMBs.

To systematically compare above batteries performance under different conditions, it can be deduced that an optimized structure of separator through fiber size regulation is indispensable towards high-performance LMBs. If the fiber size is too large such as PCF1 and PCF2, the shuttle of active materials or/and dendrite growth might be more serious to accelerate capacity loss and shorter battery life. If the fiber size is too small like PCF4, the lower porosity and electrolyte uptake rates of the separator could increase the internal resistance, leading to higher battery polarization and reduced cycling stability. When more suitable structure of separator is constructed through fiber size regulation, like PCF3, a separator with suitable pore size and distribution, good mechanical strength, higher porosity, and electrolyte uptake capacity can be achieved, thus effectively reducing polarization even at high current densities and offers optimal cycling performance during batteries running.

### 3. Conclusions

In this research, structure optimization for cellulose-based separator through fiber size regulation has been investigated systematically towards high performance lithium metal batteries (LMBs). To be specific, four types of cellulose-based separators with various fiber sizes have been constructed, and the structure-function relationship between the fiber size and the separator or battery performance, has been further studied through physicochemical structure and electrochemical performance characterizations. It can be concluded that an optimized structure of separator through fiber size regulation is indispensable towards high-performance LMBs. Specifically, the separator optimized by fiber size regulation exhibited excellent thermal stability (stable under 180 °C), good mechanical strength (tensile strengths, 6.0 MPa; Young's moduli, 315.9 MPa) and superior ionic conductivity (1.87 mS cm<sup>-1</sup> at room temperature). The corresponding batteries show stable Li plating/stripping (1000 hours), superior specific capacity

(149.8 mAh g<sup>-1</sup>), superb rate performance (5 C), and better long-term cycling performance. This work about fiber size regulation for cellulose-based separators provides an effective and reliable method to construct high safety and high performance LMBs.

### 4. Supporting Information

Electrochemical testing and other supplementary material are available in Supporting Materials.

### Acknowledgements

The authors would like to acknowledge the financial support from the National Natural Science Foundation of China, Pilot Group Program of the Research Fund for International Senior Scientists (No. 22250710676), the Educational Research Projects for Young and Middle-aged Teachers in Fujian Province (JZ230002), the Fujian Province Super 100 Talents Program, Fujian Province 100 Talents Program, Fujian Province Minjiang Scholar Program, and the Institute of New Energy Materials and Engineering, School of Materials Science and Engineering, Fuzhou University. We also want to acknowledge the anonymous reviewers who provided a lot of helpful suggestions to enhance this article.

### Conflict of Interests

The authors declare no competing financial interest.

### Data Availability Statement

The data that support the findings of this study are available from the corresponding author upon reasonable request.

**Keywords:** cellulose-based separators • fiber size regulation • structure optimization • lithium metal batteries

- [1] a) Y. Zheng, Y. Yao, J. Ou, M. Li, D. Luo, H. Dou, Z. Li, K. Amine, A. Yu, Z. Chen, *Chem. Soc. Rev.* **2020**, *49*, 8790–8839; b) S. Duan, L. Qian, Y. Zheng, Y. Zhu, X. Liu, L. Dong, W. Yan, J. Zhang, *Adv. Mater.* **2024**, *36*, 2314120. c) Y. Zhu, Z. Lao, M. Zhang, T. Hou, X. Xiao, Z. Piao, G. Lu, Z. Han, R. Gao, L. Nie, X. Wu, Y. Song, C. Ji, J. Wang, G. Zhou, *Nat. Commun.* **2024**, *15*; d) T. Bashir, S. Zhou, S. Yang, S. A. Ismail, T. Ali, H. Wang, J. Zhao, L. Gao, *Electrochim. Energy Rev.* **2023**, *6*, 5; e) J. Zhao, H. Liu, X. Li, *Electrochim. Energy Rev.* **2023**, *6*, 13; f) S. Xiong, H. Ke, L. Cao, Y. Wang, Q. Zhu, L. Zhong, L. Fan, F. Gu, *Frontiers in Energy* **2023**, *17*, 555–566.
- [2] a) M. Hong, Z. Wang, Z. Shi, Z. Liang, *Frontiers in Energy* **2023**, *17*, 569–584; b) J. Qin, Z. Yang, F. Xing, L. Zhang, H. Zhang, Z.-S. Wu, *Electrochim. Energy Rev.* **2023**, *6*, 9.
- [3] W. Yu, L. Shen, X. Lu, J. Han, N. Geng, C. Lai, Q. Xu, Y. Peng, Y. Min, Y. Lu, *Adv. Energy Mater.* **2023**, *13*, 2204055.
- [4] a) Y. Wen, J. Ding, J. Liu, M. Zhu, R. Hu, *Energy Environ. Sci.* **2023**, *16*, 2957–2967; b) Z. Wang, R. Pan, C. Xu, C. Ruan, K. Edström, M. Strømme, L. Nyholm, *Energy Storage Mater.* **2018**, *13*, 283–292.
- [5] a) W. Yang, Y. Liu, X. Sun, Z. He, P. He, H. Zhou, *Angew. Chem. Int. Ed.* **2024**, *63*, e202401428; b) Y. Zheng, N. Yang, R. Gao, Z. Li, H. Dou, G. Li, L. Qian, Y. Deng, J. Liang, L. Yang, Y. Liu, Q. Ma, D. Luo, N. Zhu, K. Li, X.

- Wang, Z. Chen, *Adv. Mater.* **2022**, *34*, e2203417; c) C. Yang, Q. Wu, W. Xie, X. Zhang, A. Brozena, J. Zheng, M. N. Garaga, B. H. Ko, Y. Mao, S. He, Y. Gao, P. Wang, M. Tyagi, F. Jiao, R. Briber, P. Albertus, C. Wang, S. Greenbaum, Y.-Y. Hu, A. Isogai, M. Winter, K. Xu, Y. Qi, L. Hu, *Nature* **2021**, *598*, 590–596; d) Z. Li, Y. Zheng, C. Liao, S. Duan, X. Liu, G. Chen, L. Dong, J. Dong, C. Ma, B. Yin, W. Yan, J. Zhang, *Adv. Funct. Mater.* **2024**, 2404427. <https://doi.org/10.1002/adfm.202404427>.
- [6] a) Y. Wang, J. Luo, L. Chen, J. Long, J. Hu, L. Meng, *J. Power Sources* **2021**, *482*, 228899; b) C. Cheng, R. Yang, Y. Wang, D. Fu, J. Sheng, X. Guo, *Carbohydr. Polym.* **2023**, *304*, 120489.
- [7] Z. Li, W. Wang, X. Liang, J. Wang, Y. Xu, W. Li, *J. Energy Chem.* **2023**, *79*, 92–100.
- [8] L. Sheng, L. Wang, J. Wang, H. Xu, X. He, *Chem. Commun.* **2020**, *56*, 10465–10468.
- [9] P. Ahvenainen, I. Kontro, K. Svedstrom, *Cellulose* **2016**, *23*, 1073–1086.
- [10] E. M. Dogan-Guner, G. T. Schueneman, M. L. Shofner, J. C. Meredith, *Cellulose* **2021**, *28*, 10875–10889.
- [11] W. Zhou, M. Chen, Q. Tian, J. Chen, X. Xu, C.-P. Wong, *Energy Storage Mater.* **2022**, *44*, 57–65.
- [12] X. H. Niu, J. Li, G. L. Song, Y. M. Li, T. He, *J. Mater. Sci.* **2022**, *57*, 7042–7055.
- [13] M. B. Agustin, F. Nakatsubo, H. Yano, *Carbohydr. Polym.* **2018**, *192*, 28–36.
- [14] G. Lin, Z. Bai, C. Liu, S. Liu, M. Han, Y. Huang, X. Liu, *J. Membr. Sci.* **2022**, *647*, 120262.
- [15] L. C. Battirola, D. M. Zanata, M. C. Gonçalves, *Composites Part A* **2018**, *113*, 105–113.
- [16] N. Xue, Z. Yuan, W. Wang, R. Xu, J. Xie, C. Lei, *Colloids Surf. A* **2022**, *633*, 127875.
- [17] M. Lindner, *J. Mater. Sci.* **2017**, *53*, 1–26.
- [18] P. R. Sharma, B. Q. Zheng, S. K. Sharma, C. B. Zhan, R. F. Wang, S. R. Bhatia, B. S. Hsiao, *ACS Appl. Polym. Mater.* **2018**, *1*, 3969–3980.
- [19] M. Beaumont, S. Winklehner, S. Veigel, N. Mundigler, W. Gindl-Altmutter, A. Potthast, T. Rosenau, *Green Chem.* **2020**, *22*, 5605–5609.
- [20] R. J. Pan, Z. H. Wang, R. Sun, J. Lindh, K. Edstrom, M. Stromme, L. Nyholm, *Cellulose* **2017**, *24*, 2903–2911.
- [21] Y. Xia, X. Li, J. Zhuang, Y. Yuan, W. Wang, *Carbohydr. Polym.* **2023**, *300*, 120231.
- [22] C. Zhang, L. Shen, J. Shen, F. Liu, G. Chen, R. Tao, S. Ma, Y. Peng, Y. Lu, *Adv. Mater.* **2019**, *31*, e1808338.
- [23] M. Qiao, G. Zhang, J. Deng, J. Guo, J. Zhang, *J. Mater. Sci.* **2022**, *57*, 11796–11808.
- [24] C. F. Ding, X. W. Fu, H. Li, J. Y. Yang, J. L. Lan, Y. H. Yu, W. H. Zhong, X. P. Yang, *Adv. Funct. Mater.* **2019**, *29*, 1904547.
- [25] B. Yuan, K. Wen, D. Chen, Y. Liu, Y. Dong, C. Feng, Y. Han, J. Han, Y. Zhang, C. Xia, A. Sun, W. He, *Adv. Funct. Mater.* **2021**, *31*, 2101420.

Manuscript received: June 29, 2024

Revised manuscript received: July 30, 2024

Accepted manuscript online: July 30, 2024

Version of record online: October 4, 2024